Materials Advances

ROYAL SOCIETY OF CHEMISTRY

PAPER

View Article Online
View Journal | View Issue

Check for updates

Cite this: *Mater. Adv.*, 2024, 5, 8515

Re-engineering lysozyme solubility and activity through surfactant complexation†

Jiaming Mu, [a] Leran Mao, [b] Gavin P. Andrews [a] and Sheiliza Carmali *[a]

Hydrophobic ion-pairing is an established solubility engineering technique that uses amphiphilic surfactants to modulate drug lipophilicity and facilitate encapsulation in polymeric and lipid-based drug delivery systems. For proteins, surfactant complexation can also lead to unfolding processes and loss in bioactivity. In this study, we investigated the impact of two surfactants, sodium dodecyl sulphate (SDS) and dioctyl sulfosuccinate (DOSS) on lysozyme's solubility, activity, and structure. SDS and DOSS were combined with lysozyme at increasing charge ratios (4 : 1, 2 : 1, 1 : 1, 1 : 2 and 1 : 4) *via* hydrophobic ion pairing at pH 4.5. Maximum complexation efficiency at the 1 : 1 charge ratio was confirmed by protein quantitation assays and zeta potential measurements, showing a near neutral surface charge. Lysozyme lipophilicity was successfully increased, with log *D* *n*-octanol/PBS values up to 2.5 with SDS and 1.8 with DOSS. Bioactivity assays assessing lysis of *M. lysodeikticus* cell walls showed up to a 2-fold increase in lysozyme's catalytic ability upon complexation with SDS at ratios less than stoichiometric, suggesting favourable mechanisms of stabilisation. Secondary structural analysis using Fourier-transform infrared spectroscopy indicated that lysozyme underwent a partial unfolding process upon complexation with low SDS concentrations. Molecular dynamic simulations further confirmed that at these low concentrations, a positive conformation was obtained with the active site residue Glu 35 more solvent-exposed. Combined, this suggested that sub-stoichiometric SDS altered the active site's secondary structure through increased backbone flexibility, leading to higher substrate accessibility. For DOSS, low surfactant concentrations retained lysozyme's native function and structure while still increasing the protein's lipophilic character. Our research findings demonstrate that modulation of protein activity can be related to surfactant chemistry and that controlled ion-pairing can lead to re-engineering of lysozyme solubility, activity, and structure. This has significant implications for advanced protein applications in healthcare, particularly towards the development of formulation strategies for oral biotherapeutics.

Received 16th July 2024,
Accepted 30th September 2024

DOI: 10.1039/d4ma00720d

rsc.li/materials-advances

Open Access Article. Published on 01 Oktober 2024. Downloaded on 16/03/2026 01.32.53.
This article is licensed under a Creative Commons Attribution 3.0 Unported Licence.

Introduction

Protein therapeutics have revolutionised the treatment of cancer, infectious diseases, and various metabolic disorders. More than 40 years after the approval of Humulin, the first clinically approved therapeutic protein, protein-based pharmaceuticals now account for two-thirds of the top-selling drugs.[1,2] In 2023, leading the sales were Keytruda (pembrolizumab, Merck) used in cancer immunotherapy and the glucagon-like peptide-1 (GLP-1) receptor agonist Ozempic (semaglutide, Novo Nordisk).[2] Despite growing success, more than 90% of biotherapeutics are still administered parenterally.[3,4] Although effective, frequent injections can be inconvenient and painful, thereby impacting patient compliance. Additionally, parenteral administration often involves higher healthcare costs due to the need for trained medical personnel. Clinical translation of oral biotherapeutics remains a significant challenge due to poor intestinal absorption and enzymatic instability in the gastrointestinal tract.[5,6] A notable example is Rybelsus (Novo Nordisk), an oral formulation of semaglutide with a bioavailability of $<1\%$, further highlighting the obstacles in developing oral protein formulations.[7,8]

One approach favoured for successful development of oral biotherapeutics is the use of lipid-based nanocarriers, including liposomes, self-emulsifying drug delivery systems, solid lipid nanoparticles and nanostructured lipid carriers.[6,9–11] These lipid-based formulations protect proteins from enzymatic degradation, improve their transmucosal transport and provide controlled release. Ongoing research within this landscape has resulted in the approval of oral peptide drugs such as Neoral (cyclosporine A, Novartis) and Mycapssa (octreotide, Chiasma), with several more currently under clinical evaluation.[9,12,13]

[a] *School of Pharmacy, Queen's University Belfast, BT9 7BL, UK. E-mail: s.carmali@qub.ac.uk*
[b] *Department of Chemical Engineering, Carnegie Mellon University, Pittsburgh, Pennsylvania, 15213, USA*

† Electronic supplementary information (ESI) available. See DOI: https://doi.org/10.1039/d4ma00720d

© 2024 The Author(s). Published by the Royal Society of Chemistry

Open Access Article. Published on 01 Oktober 2024. Downloaded on 16/03/2026 01.32.53.
This article is licensed under a Creative Commons Attribution 3.0 Unported Licence.

To facilitate the solubilisation (or encapsulation) of hydrophilic proteins into lipid-based carriers, hydrophobic ion-pairing (HIP) is often employed to enhance protein lipophilicity.[14–16] At a molecular level, HIP involves the stoichiometric association between the protein's ionisable groups (*e.g.*, basic amino acids, such as lysine or arginine residues) with oppositely charged surfactants at a suitable pH. The increased lipophilicity stems from the reversible neutralisation of the protein's charge and is dependent on surfactant chemistry and structure. For example, sulphonate- and sulphate-based surfactants have been shown to substantially increase the lipophilicity of insulin, bovine serum albumin and horseradish peroxidase.[17] In addition to the surfactant headgroup, the structure and flexibility of the hydrophobic tail are also important factors, with rigid alkyl moieties resulting in lower protein lipophilicity enhancements in contrast to more flexible, linear surfactant analogues. Pre-clinical studies have also shown that surfactant type impacts oral bioavailability, with increased lipophilicity leading to improved intestinal absorption.[18]

Paradoxically, surfactant complexation can also lead to unfavourable unfolding processes, which disrupt the protein's structure and lead to a loss of bioactivity and reduced therapeutic efficacy.[19] Electrostatic and hydrophobic interactions drive surfactant complexation, with the mode and strength of these interactions resulting in altered protein structures and dynamics, and consequently, function.[20] Above the surfactant's critical micellar concentration (CMC), hydrophobic interactions dominate, causing proteins to unfold. However, at surfactant concentrations similar to those used in HIP, complexation can yield protein conformations with favourable activities and/or stabilities. We hypothesised that by adjusting the type and concentration of surfactants during the HIP process, we can achieve a spectrum of protein structures, each with its own customised lipophilicity and activity characteristics.

In this study, we investigated the impact of two anionic surfactants, sodium dodecyl sulphate (SDS) and dioctyl sulfosuccinate (DOSS) on the structure and activity of lysozyme. Lysozyme, an antimicrobial enzyme, and an important component of the innate immune system, has been commonly used in formulation studies, including for hydrophobic ion pairing. It has a well characterised three-dimensional structure and an established enzymatic assay.[21–23] These factors make lysozyme an ideal model to unravel the effects of surfactant complexation on protein structure and function. Initially, we ion-paired lysozyme with either SDS or DOSS at increasing surfactant concentrations. We then assessed the lipophilic properties of the resulting complexes using a shake-flask method. The catalytic activity of lysozyme and lysozyme-surfactant complexes was measured using a *M. lysodeikticus* cell wall degradation assay. We then correlated activity data with changes to lysozyme's secondary structure, as determined by Fourier-Transform Infrared Spectroscopy (FT-IR), and thermal resistance, as measured by differential scanning calorimetry (DSC). To gain further insight, we compared wet-lab findings with molecular dynamic simulations. These simulations were performed with lysozyme and lysozyme-surfactant complexes at surfactant concentrations that produced optimal lipophilicity and activity profiles.

Experimental

Materials

Lysozyme from chicken egg white (lyophilized powder, protein ≥90%, ≥20 000 units per mg dry weight), Micro BCA™ Protein Assay Kit and dimethylsulfoxide (DMSO) were purchased from ThermoFisher Scientific (United Kingdom). *Micrococcus lysodeikticus* lyophilized cells, sodium dodecyl sulphate (SDS), dioctyl sulfosuccinate (DOSS), sodium acetate, acetic buffer ≥ 99%, potassium phosphate monobasic and dibasic solutions, and phosphate buffered saline (PBS) tablets were obtained from Sigma-Aldrich. All chemicals were used without further purification. Buffers were filtered through 0.2 μm polyethersulfone (PES) membrane before use. Deionized water was used for all the experiments.

Lysozyme-surfactant ion-pairing process

Lysozyme solution (5 mg mL^{-1}, as determined by spectrophotometry at 280 nm, $\varepsilon^{1\%}_{280}$ 26.4[24]) was prepared with 10 mM acetate buffer pH 4.5 to achieve a net positive charge and maximum complexation efficiency (Fig. S1, ESI†). SDS was dissolved in deionised water (20 mg mL^{-1}) while DOSS was prepared as an aqueous solution with 2% DMSO (15 mg mL^{-1}) to ensure sufficient solubilisation. Surfactant aqueous solutions (1 mL) were then added, dropwise at room temperature, to the lysozyme solution, to achieve the desired surfactant: lysozyme ratios (Table 1) in separate vessels and allowed to mix for 20 min at 550 rpm (Eppendorf 5382 ThermoMixer C v.3.5.0).

White precipitates in solution indicated HIP complexation. Complexes were recovered by centrifugation of cloudy solution at 13 500 rpm for 10 min at 4 °C (AXYSPIN Refrigerated microcentrifuge). The obtained precipitates were washed with deionised water, followed by lyophilisation (Edwards Modulyo Freeze Dryer) and stored at −20 °C.

Complexation efficiency (CE) was determined by quantification of non-complexed lysozyme in supernatant with MicroBCA assay (Table S1, ESI†) and eqn (1):

$$\mathrm{CE}\,(\%) = 100 \times \left(1 - \frac{C_{\text{lysozyme after ion-pairing}}}{C_{\text{lysozyme before ion-pairing}}}\right) \qquad (1)$$

Characterisation of lysozyme-surfactant complexes

Zeta potential determination. Zeta potential measurements were conducted according to previously described methodology by Griesser and co-workers.[16] Native lysozyme and lysozyme-surfactant

Table 1 Surfactant concentration, molar and charge ratios used for lysozyme ion-pairing in this study (lysozyme 5 mg mL^{-1})

	Lysozyme : surfactant	
Surfactant (mM)	Molar ratio	Charge ratio
0.8	4 : 9	8 : 1
1.6	2 : 9	4 : 1
3.1	1 : 9	2 : 1
6.3	1 : 18	1 : 1
12.5	1 : 36	1 : 2
25.0	1 : 72	1 : 4

© 2024 The Author(s). Published by the Royal Society of Chemistry

Open Access Article. Published on 01 Oktober 2024. Downloaded on 16/03/2026 01.32.53. This article is licensed under a Creative Commons Attribution 3.0 Unported Licence.

complexes were prepared at 10 mg mL^{-1}, filtered using 0.45 μm hydrophilic polytetrafluoroethylene (PTFE) syringe filters, and measured by laser Doppler micro-electrophoresis using a Zetasizer NanoZS (Malvern Instruments, UK). Samples were measured in triplicate at 25 °C. Data was analysed with Prism 10.2.3., with zeta potential values plotted against surfactant concentration.

Determination of log *D*. Distribution studies using 1-octanol and PBS was adapted from Phan and co-workers.[25] 1-Octanol was saturated with PBS by mixing of both solvents for 24 hours at 25 °C. After this time, the organic phase was separated by centrifugation under 4000 rpm for 20 min (SIGMA® Laboratory Centrifuge 6–15H). Each lysozyme-surfactant complex (1 mg) was dissolved in 500 μL of PBS saturated 1-octanol. Subsequently, the same volume of the PBS aqueous phase was added to the organic phase, after which the mixture was mixed at 550 rpm for 3 hours at 4 °C. After this time, aqueous and organic phases were separated by centrifugation at 13 500 rpm for 10 min. Lysozyme concentration in the aqueous phase was determined by Micro BCA assay and the partition coefficient log *D* was determined based on eqn (2):

$$\log D_{1-\text{octanol/PBS}} = \log \frac{C_{\text{lysozyme in}-\text{octanol}}}{C_{\text{lysozyme in PBS}}} \quad (2)$$

Lysozyme activity assay. Lysozyme activity was measured by the lysis of *Micrococcus lysodeikticus* cell walls.[21] Absorption at 450 nm of suspended *M. lysodeikticus* (800 μL, 0.3 mg mL^{-1}) in 50 mM phosphate buffer, pH 6.5 was measured by UV spectroscopy (Thermo Scientific Multiskan SkyHigh Microplate Spectrophotometer) at room temperature. Native lysozyme or dissociated lysozyme (80 μL, 0.35 μM in 50 mM phosphate buffer, pH 6.5; Fig. S2, ESI†) was added and the change in absorbance at 450 nm at room temperature was monitored.

Fourier transform infrared spectroscopy (FTIR). Lysozyme-surfactant complexes (0.35 mM lysozyme solution; surfactant concentration 1.6–12.5 mM) were scanned between 4000–650 cm^{-1} with a diamond attenuated total reflectance FTIR (Agilent Technologies Cary 630 FTIR). Native lysozyme was performed as control.

The inverted second-derivative spectra were obtained from the derivative function of peak analysis and fitted with Gaussian band profiles[26] with OriginPro 2023b. The fraction of α-helix in infrared second-derivative amide spectra was determined by computing the area of the component peak divided by the sum of areas of all the component peaks of the amide I band around 1650 cm^{-1}.

Steady-state fluorescence measurements. Fluorescence (HITACHI F02710 fluorescence spectrophotometer) was measured as previously described.[19] The excitation was set at 290 nm with the emission range between 300–500 nm. Both excitation and emission slits widths were set at 5 nm. Measurements were performed in a 10 mm quartz cuvette at room temperature. The emission wavelength and tryptophan intensity were tested for lysozyme-surfactant complex suspensions and protein concentration was kept constant at 5 mg mL^{-1} for all the samples. Native lysozyme was used as negative control.

Differential scanning calorimetry (DSC). To investigate the impact of surfactant complexation on lysozyme thermal stability, the melting temperature of complexes and native lysozyme was determined using differential scanning calorimetry. DSC measures the change of enthalpy of protein that is initially in its native conformation. The mass (mg) of empty and sample-containing DSC aluminium pans were weighed and recorded, after which they were placed on the TA ® DSC Q20 (Table S2, ESI†). Each pan was kept isothermal at −20 °C for 10 min before a 10 °C min^{-1} ramp to 200 °C. The melting point of each endothermic peak was analysed with OriginPro 2023b. Samples were measured in triplicate and results were plotted with Prism 10.2.3.

Scanning electron microscopy (SEM). Scanning electron microscopy (HITACHI TM3030 Tabletop Microscope) was used to visualise the morphological features of lyophilized lysozyme-surfactant complexes. The images of freeze-dried powers, including complex and dissociated lysozyme were taken on a vacuum stage at an accelerating voltage of 25 KV. Native lysozyme was performed as comparison.

Molecular dynamics simulations

The starting structure for lysozyme was obtained from the protein data bank (PDB ID 6LYZ). Protein protonation at pH 6.5 was determined using PDB2PQR continuum electrostatics.[27] Surfactant structures were built in Avogadro and energy-minimized using the universal force field. Lysozyme was modelled with the CHARMM C36m force field with WYF parameters for cation–pi interactions using CHARMM GUI in a water box fitted to the protein size (~66–68 Å).[28–30] SDS and DOSS topology files were generated using CGenFF parameters.[31,32] Protein structures were solvated with TIP3 explicit solvent, and the system was neutralized using 50 mM K^+ and PO_3^{2-} ions to better represent experimental settings.

Molecular dynamic simulation was run on GROMACS 2020.1.[33,34] The protein structure was energy minimized using the steepest descent approach consisting of 5000 steps followed by NVT equilibration with Nose–Hoover temperature coupling for 125 ps. Simulations for lysozyme with and without the addition of surfactant were run for 35 ns with an NPT ensemble using Nose–Hoover temperature coupling and Parrinello–Rahman isotropic pressure coupling at 293.15 K. Electrostatics were modelled using the Particle Mesh Ewald method in an automatically generated grid. The production run was analysed for root-mean-squared deviation (RMSD) and radial probability distribution ($G(r)$) using VMD.[35] The averaged PDB structure in each 5 ns simulation sequence was exported and visualized in Biovia Discovery Studio (Dassault Systems) for secondary structure analysis and solvent-accessible surface area (SASA) analysis (ESI†).

Results and discussion

Preparation and characterisation of lysozyme-surfactant complexes

Lysozyme is a small globular protein consisting of 129 amino acids cross-linked with four disulphide bridges.[22] Due to its high isoelectric point (pI 11.35), lysozyme's acidic groups

Open Access Article. Published on 01 Oktober 2024. Downloaded on 16/03/2026 01.32.53.
This article is licensed under a Creative Commons Attribution 3.0 Unported Licence.

(7 aspartic acid and 2 glutamic acid residues) remain non-ionised and its basic groups (11 arginine, 1 histidine and 6 lysine residues) become protonated at low pH. As a result, these 18 positively charged residues can non-covalently interact with negatively charged surfactants (Fig. 1A and B). In this study, lysozyme was ion paired with anionic sodium dodecyl sulphate (SDS) and dioctyl sulfosuccinate (DOSS) at pH 4.5. These two surfactants were selected due to their similar, stabilising kosmotropic headgroups (SO_4^- and SO_3^-, respectively) and distinct hydrophobic, tail groups (linear *vs.* branched).

Complexation efficiency. The gradual addition of SDS and DOSS to the lysozyme solution increased its turbidity and led to the formation of precipitates due to surfactant complexation. We observed maximum complexation efficiency at the stoichiometric charge ratio 1 : 1 (Fig. 1C). At this ratio, we expected 18 surfactant molecules to bind to 1 lysozyme molecule, which corresponds to a surfactant concentration of 6.3 mM. When surfactant concentration exceeds this binding saturation point, micelles form, and proteins can be re-solubilised.[37] We experimentally determined the CMC values for SDS and DOSS under the conditions used in this study and found them to be 7.2 and 4.8 mM, respectively (Fig. S3 and S4, ESI†). This further confirmed that the observed decrease in both complexation efficiency and solution turbidity above the surfactant concentration of 6.3 mM led to protein re-solubilisation. Dynamic light scattering experiments also showed that complexes with surfactant concentration, namely at the 1 : 4 charge ratio, were found to have similar particle sizes to native lysozyme (Table S1, ESI†). These results are also in agreement with previous studies that have shown that a stoichiometric or slightly higher binding ratio is optimal for hydrophobic ion pairing.[16]

Both SDS and DOSS have negatively charged head groups that can interact ionically with the basic residues of lysozyme, as shown in Fig. 1B. However, SDS and DOSS have distinct chemical and structural properties. SDS has a linear structure, while DOSS is a branched and more lipophilic surfactant, with log *P* 3.86 and 4.36, respectively (calculated by ALOGPS 2.1).[36] We hypothesized that these chemical and structural differences would affect how the surfactants interact with the surface of lysozyme, with DOSS involving more hydrophobic interactions. To further understand this, we used zeta potential as a proxy for surface charge. We noted a decreasing trend with increasing surfactant concentration for both SDS and DOSS, as shown in Fig. 1D This trend suggests that the primary mode of interaction for both surfactants is ionic. At the stoichiometric binding point, we observed an apparent charge neutralisation effect due to near complete complexation at all positively charged residues of lysozyme. Beyond this point, an overall negative surface charge was observed, attributed to the presence of excess anionic surfactants.

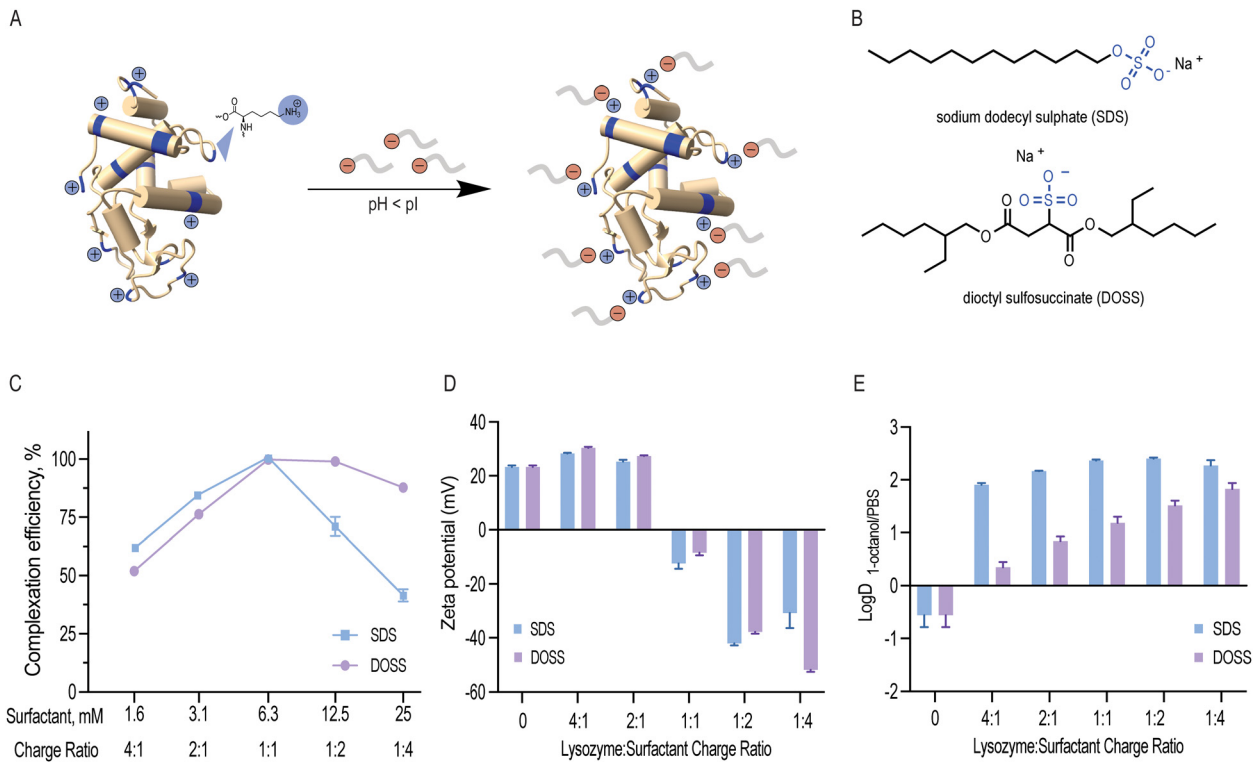

Fig. 1 (A) At low pH conditions, lysozyme is positively charged and can associate with anionic surfactants primarily through non-covalent electrostatic interactions, forming lysozyme-surfactant complexes; (B) chemical structures of surfactants sodium dodecyl sulphate (SDS) and dioctyl sulfosuccinate (DOSS) used in this study; (C) impact of surfactant concentration on lysozyme-surfactant complexation efficiency; (D) apparent surface charge variation as a function of lysozyme: surfactant charge ratio; (E) impact of lysozyme: surfactant charge ratio on lysozyme hydrophobicity as determined by the partition coefficient (log *D*) of lysozyme following surfactant addition.

© 2024 The Author(s). Published by the Royal Society of Chemistry

Open Access Article. Published on 01 Oktober 2024. Downloaded on 16/03/2026 01.32.53.
This article is licensed under a Creative Commons Attribution 3.0 Unported Licence.

Lipophilic properties. We next determined the partitioning of the prepared lysozyme-surfactant complexes in a 1-octanol/PBS system to confirm their enhanced lipophilic character (Fig. 1E). The solubility of free lysozyme in 1-octanol was initially 1.0 mg mL^{-1}, which increased nearly three-fold when bound with SDS. For lysozyme-DOSS complexes, an increase in lipophilicity was also observed, although to a lesser extent. Prud'homme and researchers, have previously reported that counterions with higher molecular weight, hydrophobicity, and stronger acidity (lower pK_a values) facilitate the ion-pairing process.[38] We anticipated that the complexation with DOSS, due to its higher lipophilicity and size, would augment lysozyme lipophilicity further than SDS. However, predicted pK_a values indicated that the stronger acidic form of SDS (pK_a −3.50) in comparison to DOSS (pK_a 0.1) allowed for stronger ionic interactions, forming stronger complexes, and consequently, with increased lipophilicity.[39] Both surfactants were, however, able to effectively increase the hydrophobic character of lysozyme.

Morphology changes. We also investigated the impact of hydrophobic ion-pairing on the shape and size of lysozyme using scanning electron microscopy. From SEM analysis, we observed that native lysozyme initially displayed a spherical and smooth shape (Fig. 2A). In contrast, complexes formed with SDS or DOSS at the 1 : 1 charge ratio, as shown in Fig. 2B and C, exhibited a more rigid and rough surface texture. Moreover, upon surfactant dissociation, we noted that this rigidity was maintained, indicating that surfactant complexation had irreversibly altered lysozyme's morphology (Fig. 2D and E).

Impact of surfactant complexation on lysozyme bioactivity

An important aspect of hydrophobic ion pairing with proteins is to ensure functional integrity. During complexation, lysozyme precipitation may result in enzyme deactivation due to irreversible aggregation. Moreover, ionic surfactants, such as SDS and DOSS, are usually associated with protein denaturation due to their charged head groups, but in some cases, they can heighten activity, where partially unfolded proteins retain their overall native shape, and consequently function.[40]

To investigate how surfactant complexation impacted lysozyme function, we measured lysozyme's activity *via* bacterial cell wall lysis, following surfactant dissociation (Fig. 3A). For both SDS and DOSS, lysozyme showed a catalytic enhancement at low surfactant concentrations. For lysozyme-SDS complexes, a near two-fold enhancement was observed when a maximum of 9 surfactant molecules were bound to 1 molecule of lysozyme (0.8–3.1 mM SDS concentration). For DOSS complexes, this increase in activity was less accentuated. At higher concentrations, complexes formed with SDS and DOSS led to a loss in activity. This can be attributed to protein unfolding due to micelle formation and the loss of lysozyme's positive charge in the active site, leading to alterations in substrate recognition.

To better understand whether the observed heightened activity was a result of surfactant presence or ion-pairing, we conducted control studies measuring the activity of non-complexed lysozyme in the presence of SDS and DOSS at a concentration of 1.6 mM, or 4 : 1 ratio (Fig. 3B). We selected this surfactant concentration as these complexes displayed similar activity profiles. Results showed that the activity of pre-formed SDS complexes (L-SDS) was significantly different from that of native lysozyme (L) and lysozyme in the presence of SDS (C-SDS). This indicated that ion-pairing with 1.6 mM SDS, and the subsequent increase in activity, was due to surfactant complexation which may have induced positive conformational changes. In contrast, for the DOSS complex (L-DOSS), no

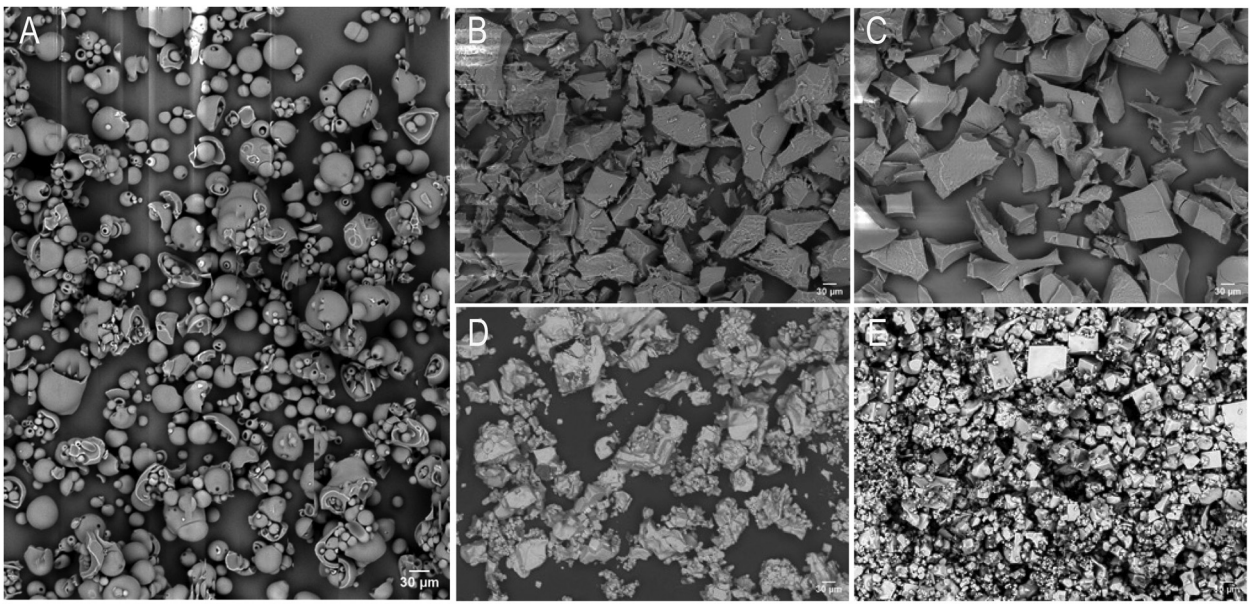

Fig. 2 (A) SEM image of Native lysozyme; (B) L-SDS complex at the charge ratio of 1 : 1; (C) L-DOSS complex at the charge ratio of 1 : 1; (D) dissociated lysozyme from the L-SDS complex; (E) dissociated lysozyme from the L-DOSS complex. Sample was freeze-dried before testing at the magnitude of 250×. Images were processed with Fiji ImageJ 1.54 h.

Open Access Article. Published on 01 Oktober 2024. Downloaded on 16/03/2026 01.32.53.
This article is licensed under a Creative Commons Attribution 3.0 Unported Licence.

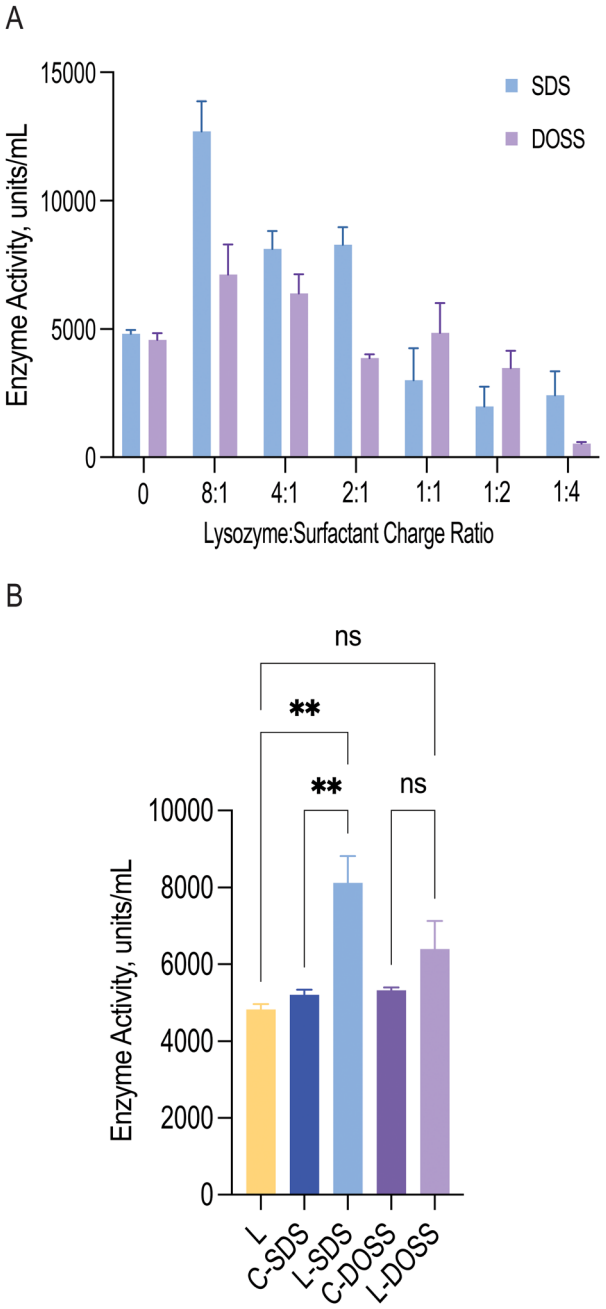

Fig. 3 (A) Impact of SDS and DOSS concentration on lysozyme lytic activity; (B) comparative study between native lysozyme (L), lysozyme pre-complexed with 1.6 mM SDS or DOSS (L-SDS and L-DOSS 4 : 1, respectively) and control samples with lysozyme in the presence of 1.6 mM SDS or DOSS (C-SDS and C-DOSS, respectively). Shown are three individual experiments ± SEM. *$p < 0.05$ by ordinary one-way ANOVA (Šidák's multiple comparisons test).

statistically significant difference was observed between native lysozyme (L) and lysozyme in the presence of 1.6 mM DOSS (C-DOSS). This suggested DOSS complexation did not impact lysozyme's catalytic activity, retaining its original native function. Previous reports have shown that the increase in lysozyme's bioactivity can be related to increased hydrophobic interactions between lysozyme and the cell substrate.[41] Our findings are consistent with these reports, with SDS complexes showing increased lipophilicity and activity properties.

To gain further insight into the source of lysozyme's catalytic enhancement upon surfactant addition, we used molecular dynamics (MD) to simulate our experimental system with 9 molecules of either SDS or DOSS interacting with lysozyme at pH 6.5. Analysis of the MD trajectory showed a higher degree of backbone flexibility of the active site residues throughout the simulation time, particularly for SDS molecules. Conformational flexibility has been shown to correlate strongly with bioactivity, which for lysozyme may also relate to increased substrate access.[42]

Increasing protein hydrophobicity can also lead to partial unfolding, with lysozyme's active site residues Glu 35 and Asp 52 slightly more solvent-exposed, contributing to an apparent catalytic enhancement.[43] Solvent accessibility calculations showed that lysozyme with 9 molecules of surfactant led to an increase in exposure of Glu 35 but not for Asp 52, suggesting the enhanced activity effect primarily stemmed from conformational changes in Glu 35. A closer analysis revealed that at the 2 : 1 lysozyme : surfactant charge ratio complex, Glu 35 was predominately located in a β-turn secondary structure, while complexes with charge ratios where activity was lost, an α-helix structure was observed. The β-turn structure has been shown to increase protein stability and dynamics and increased solvent exposure.[44] Interestingly, no difference in secondary structure was observed for the catalytic residue Asp 52. Combined, these findings suggest that sub-stoichiometric concentrations of SDS likely altered the secondary structure of the lysozyme active site by modulating the active site's backbone flexibility, leading to higher substrate accessibility.

Impact of surfactant interactions on lysozyme structure

After determining how the catalytic activity of lysozyme varies with surfactant type and concentration, we now sought to explore how the structure of lysozyme changes upon hydrophobic ion-pairing. We first used FTIR spectroscopy to investigate changes to lysozyme's secondary structure upon surfactant association. We focused on analysis of the amide I band (1600–1700 cm^{-1}), which is due to C=O stretching vibrations of peptide bonds and is influenced by the secondary structure.[45]

As shown in Fig. 4A, both SDS and DOSS association led to distinct modifications in lysozyme's secondary structure. For SDS, lysozyme complexes initially underwent a partial unfolding process, as observed by a decrease in α-helical content. This was followed by an increase in helical structure at higher surfactant concentrations.

Quantitative analysis of the deconvoluted amide I band revealed that the native lysozyme contained approximately 41.8% α-helix content, which increased to 57.3% in the presence of excess SDS. This observation aligns with previous studies, where SDS binding has been found to induce a molten globule state, characterised by high α-helical content but lack of tertiary structure.[46]

In contrast, lysozyme-DOSS complexes at low surfactant concentrations retained their α-helical content (41.8%),

© 2024 The Author(s). Published by the Royal Society of Chemistry

Open Access Article. Published on 01 Oktober 2024. Downloaded on 16/03/2026 01.32.53.
This article is licensed under a Creative Commons Attribution 3.0 Unported Licence.

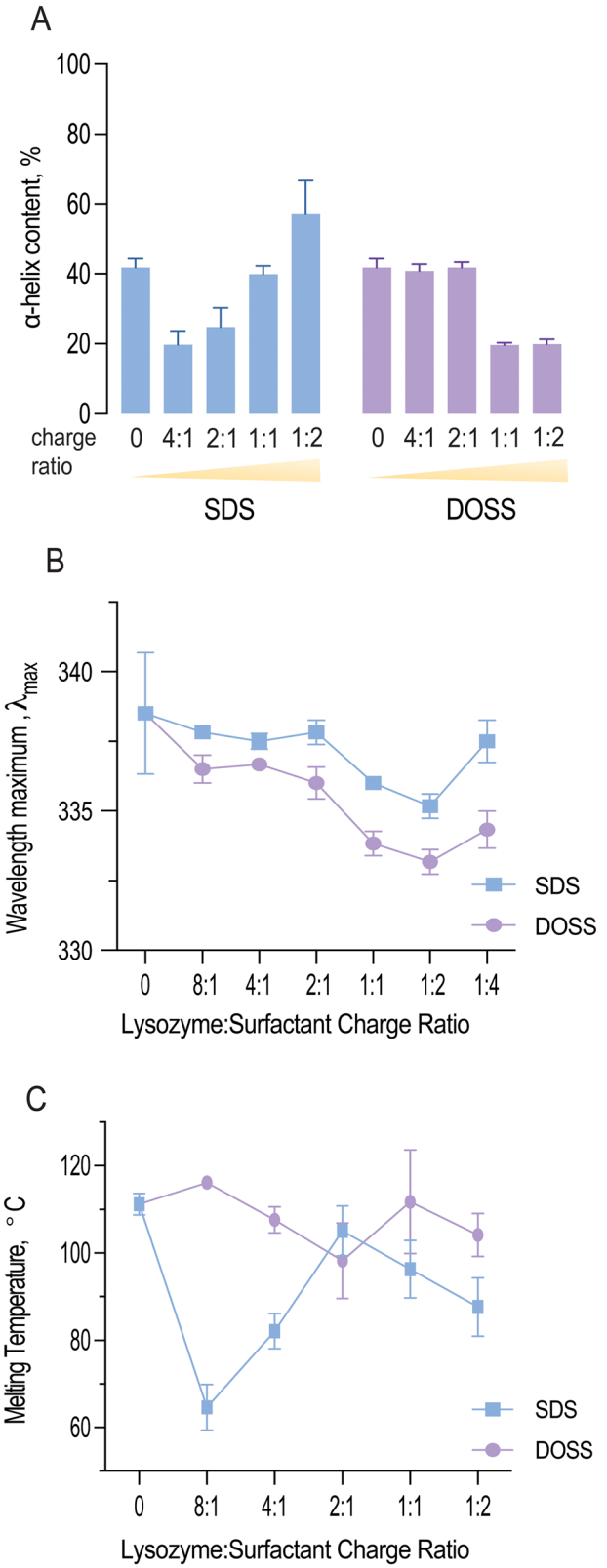

Fig. 4 (A) Impact of surfactant concentration on lysozyme secondary structure as determined by the content of α helix at amide *I* band, [Lysozyme] = 0.35 mM; (B) changes in wavelength maximum (l_{max}) of lysozyme complexes with increasing concentrations of SDS and DOSS; (C) the effect of surfactant complexation on lysozyme's thermal resistance.

possibly due to predominant electrostatic interactions between DOSS's negatively charged headgroup and lysozyme's cationic residues. However, in the presence of excess DOSS, hydrophobic interactions can also occur, which was observed by a significant loss in α-helical content (19.9%).

Analysis of the variation of intrinsic fluorescence properties of lysozyme in the presence of surfactant also provided us with some further insight into the observed conformational changes. Tryptophan fluorescence is dependent on the polarity of its local environment, with changes in wavelength maximum and fluorescence intensity roughly correlated to solvent exposure. Lysozyme contains 6 tryptophan residues, with Trp 62 and 108 responsible for most of the protein's emission.[47]

Fig. 4B shows the wavelength maximum (λ_{max}) of lysozyme at a fixed lysozyme concentration (5 mg mL^{-1}) with increasing surfactant concentrations. For both SDS and DOSS, a shift in λ_{max} was observed, further confirming the occurrence of protein conformational changes. For lysozyme-SDS complexes, the λ_{max} first underwent an increasing blue shift until reaching the 1 : 2 charge ratio or surfactant concentration up to 12.5 mM. These findings indicate that the tryptophan residues in lysozyme may have experienced a more hydrophobic microenvironment, in agreement with our complexation and lipophilicity results shown in Fig. 1C and E. Above the SDS concentration of 12.5 mM, a red shift in the wavelength maximum back to 337 nm was noted for lysozyme, corresponding to the re-solubilisation of lysozyme and SDS micellar re-folding. For lysozyme-DOSS complexes a similar trend was initially observed, albeit without the complete red shift in the presence of excess surfactant, suggesting that DOSS leads to a distinct unfolding pathway, without the formation of a molten globule state.

Impact of surfactant complexation on lysozyme thermal stability

Previous studies have established a connection between protein stability, thermal resistance, and factors such as protein electrostatics, hydropathy and core packing.[48] Hyperthermophilic proteins are characterised by enhanced hydrophobic interactions and salt bridge formations which are important in their ability to withstand elevated temperatures.[49] Since surfactant complexation increased lysozyme's hydrophobicity, we now aimed to understand the impact on lysozyme's thermal stability. We characterised lysozyme and resulting complexes' thermal properties using differential scanning calorimetry, and analysed thermal resistance as defined by the melting temperature (T_m).

Fig. 4C illustrates how the melting temperature of lysozyme fluctuates with the concentration of SDS and DOSS. Typically, a higher T_m value indicates a more stable protein structure.[50] In the case of lysozyme-SDS complexes, a significant drop in the melting temperature was noted initially. However, this was followed by a rise at the 2 : 1 charge ratio (or 3.1 mM), bringing it close to the original melting temperature of native lysozyme (T_m = 111.23 ± 2.5 °C). Subsequently, we observed a slow decline in thermal resistance. Previous studies have demonstrated a connection between protein helicity and thermal stability.[51] A detailed examination of the variations in thermal

Open Access Article. Published on 01 Oktober 2024. Downloaded on 16/03/2026 01.32.53.
This article is licensed under a Creative Commons Attribution 3.0 Unported Licence.

resistance and helical content in lysozyme-SDS complexes indeed confirms this correlation. The initial decrease in helicity coincides with the same concentration range as the reduction in lysozyme's melting temperature. Upon reaching an SDS concentration of 3.1 mM, we observed an increase in thermal resistance, which corresponds with the rise in helical content due to SDS-induced helical folding.

Furthermore, we noted that the initial decline in thermal stability was linked to an increase in lysozyme's catalytic activity. SDS has been shown to stabilize the β- strand secondary structure at low concentrations.[52] Our MD studies revealed that the active site residue, Glu 35, was in a β-turn secondary structure at concentrations where lysozyme remained functional and analysis of lysozyme-surfactant interactions showed that in contrast to DOSS, SDS displayed less contacts with residues located in β-turns, which are important for stability. Therefore, we hypothesise that at sub-stoichiometric ratios, SDS enhances lysozyme's catalytic activity while reducing its thermal stability, exemplifying a typical 'stability-activity trade-off'.

Analysis of thermal resistance of lysozyme-DOSS complexes showed a subtle stabilisation effect at the 8 : 1 charge ratio. This was subsequently followed by a steady decrease, reaching its minimum at the 2 : 1 charge ratio. After this point, we observed an increase in the melting temperature, which remained close to the original T_m of native lysozyme. As mentioned previously, changes in protein solubility can often suggest a variation in the protein's melting temperature. For lysozyme complexes with DOSS, lipophilic and T_m changes were less pronounced in comparison to lysozyme-SDS complexes, further highlighting the dependency of both parameters.

Conclusions

In this study, we formed ion pairs between lysozyme and two surfactants, SDS and DOSS, at various charge ratios. This resulted in a variety of lysozyme-surfactant complexes, each with unique characteristics in terms of lipophilicity, activity, and structure. Complexation with either SDS or DOSS increased lysozyme's hydrophobicity, however only the controlled addition of SDS in sub-stoichiometric amounts, below the 1 : 1 ratio, led to complexes with increased activity. This increased activity was attributed to partial unfolding and greater exposure of the active site, thereby enhancing substrate accessibility. Our study underscores that surfactant chemistry can influence protein activity and that controlled ion-pairing can modify lysozyme solubility while enhancing bioactivity. These insights are currently being applied in the development of lipid-based formulation strategies for oral biotherapeutics, potentially leading to more effective, and patient-friendly treatments.

Author contributions

Conceptualisation: S. C., and G. P. A.; data curation: J. M. and L. M.; data analysis and interpretation: S. C., J. M. and L. M.; manuscript writing/editing and visualisation: S. C., J. M. and L. M.

Data availability

Data for this article has been deposited in the Queen's University Belfast repository - Queen's University Research Portal at **https://pure.qub.ac.uk/**.

Conflicts of interest

There are no conflicts to declare.

Acknowledgements

Financial support from the Queen's University/China Scholarship Council PhD Scholarships is acknowledged.

References

1 *FDA Drug Bull.*, 1982, **12**, 18–19.
2 P. Verdin, *Nat. Rev. Drug Discovery*, 2024, **23**, 240.
3 A. Patel, K. Cholkar and A. K. Mitra, *Ther. Delivery*, 2014, **5**, 337–365.
4 R. J. Kulchar, R. Singh, S. Ding, E. Alexander, K. W. Leong and H. Daniell, *Biomaterials*, 2023, **302**, 122312.
5 H. Peng, J. Wang, J. Chen, Y. Peng, X. Wang, Y. Chen, D. L. Kaplan and Q. Wang, *Expert Opin. Drug Delivery*, 2023, **20**, 1349–1369.
6 G. Noh, T. Keum, V. Raj, J. Kim, C. Thapa, K. Shakhakarmi, M. J. Kang, Y. T. Goo, Y. W. Choi and S. Lee, *Int. J. Biol. Macromol.*, 2023, **225**, 911–922.
7 S. Hughes and J. J. Neumiller, *Clin. Diabetes Publ. Am. Diabetes Assoc.*, 2020, **38**, 109–111.
8 R. V. Overgaard, A. Navarria, S. H. Ingwersen, T. A. Bækdal and R. J. Kildemoes, *Clin. Pharmacokinet.*, 2021, **60**, 1335–1348.
9 S. Haddadzadegan, F. Dorkoosh and A. Bernkop-Schnürch, *Adv. Drug Delivery Rev.*, 2022, **182**, 114097.
10 E. Muntoni, E. Marini, N. Ahmadi, P. Milla, C. Ghè, A. Bargoni, M. T. Capucchio, E. Biasibetti and L. Battaglia, *Acta Diabetol.*, 2019, **56**, 1283–1292.
11 J. Mudassir, A. Raza, M. A. Khan, H. Hameed, G. A. Shazly, A. Irfan, S. J. Rana, K. Abbas, M. S. Arshad, S. Muhammad and Y. A. Bin Jardan, *Pharmaceutics*, 2023, **15**, 1973.
12 N. Parquet, O. Reigneau, H. Humbert, M. Guignard, P. Ribaud, G. Socié, A. Devergie, H. Espérou and E. Gluckman, *Bone Marrow Transplant.*, 2000, **25**, 965–968.
13 A. Labadzhyan, L. B. Nachtigall, M. Fleseriu, M. B. Gordon, M. Molitch, L. Kennedy, S. L. Samson, Y. Greenman, N. Biermasz, M. Bolanowski, A. Haviv, W. Ludlam, G. Patou and C. J. Strasburger, *Pituitary*, 2021, **24**, 943–953.
14 J. D. Meyer and M. C. Manning, *Pharm. Res.*, 1998, **15**, 188–193.
15 K. D. Ristroph and R. K. Prud'homme, *Nanoscale Adv.*, 2019, **1**, 4207–4237.
16 J. Griesser, G. Hetényi, M. Moser, F. Demarne, V. Jannin and A. Bernkop-Schnürch, *Int. J. Pharm.*, 2017, **520**, 267–274.

© 2024 The Author(s). Published by the Royal Society of Chemistry

Open Access Article. Published on 01 Oktober 2024. Downloaded on 16/03/2026 01.32.53.
This article is licensed under a Creative Commons Attribution 3.0 Unported Licence.

17 V. Claus, M. Sandmeier, N. Hock, H. Spleis, S. Lindner, M. Kalb and A. Bernkop-Schnürch, *Int. J. Pharm.*, 2023, **647**, 123507.
18 S. Bonengel, M. Jelkmann, M. Abdulkarim, M. Gumbleton, V. Reinstadler, H. Oberacher, F. Prüfert and A. Bernkop-Schnürch, *J. Controlled Release*, 2018, **273**, 21–29.
19 Y. Sun, P. L. O. Filho, J. C. Bozelli, J. Carvalho, S. Schreier and C. L. P. Oliveira, *Soft Matter*, 2015, **11**, 7769–7777.
20 M. D. Lad, V. M. Ledger, B. Briggs, R. J. Green and R. A. Frazier, *Langmuir*, 2003, **19**, 5098–5103.
21 A. N. Smolelis and S. E. Hartsell, *J. Bacteriol.*, 1949, **58**, 731–736.
22 L. N. Johnson, *Sci. Prog.*, 1966, **54**, 367–385.
23 A. A. A. Hassan, T. Sovány, K. Pamlényi, M. Deák, V. Hornok, E. Csapó, G. Regdon, I. Csóka and K. Kristó, *Pharmaceutics*, 2024, **16**, 589.
24 K. C. Aune and C. Tanford, *Biochemistry*, 1969, **8**, 4579–4585.
25 T. N. Q. Phan, R. Ismail, B. Le-Vinh, S. Zaichik, F. Laffleur and A. Bernkop-Schnürch, *ACS Biomater. Sci. Eng.*, 2020, **6**, 5032–5039.
26 A. Dong, P. Huang and W. S. Caughey, *Biochemistry*, 1990, **29**, 3303–3308.
27 E. Jurrus, D. Engel, K. Star, K. Monson, J. Brandi, L. E. Felberg, D. H. Brookes, L. Wilson, J. Chen, K. Liles, M. Chun, P. Li, D. W. Gohara, T. Dolinsky, R. Konecny, D. R. Koes, J. E. Nielsen, T. Head-Gordon, W. Geng, R. Krasny, G.-W. Wei, M. J. Holst, J. A. McCammon and N. A. Baker, *Protein Sci. Publ. Protein Soc.*, 2018, **27**, 112–128.
28 S. Jo, T. Kim, V. G. Iyer and W. Im, *J. Comput. Chem.*, 2008, **29**, 1859–1865.
29 B. R. Brooks, C. L. Brooks, A. D. MacKerell, L. Nilsson, R. J. Petrella, B. Roux, Y. Won, G. Archontis, C. Bartels, S. Boresch, A. Caflisch, L. Caves, Q. Cui, A. R. Dinner, M. Feig, S. Fischer, J. Gao, M. Hodoscek, W. Im, K. Kuczera, T. Lazaridis, J. Ma, V. Ovchinnikov, E. Paci, R. W. Pastor, C. B. Post, J. Z. Pu, M. Schaefer, B. Tidor, R. M. Venable, H. L. Woodcock, X. Wu, W. Yang, D. M. York and M. Karplus, *J. Comput. Chem.*, 2009, **30**, 1545–1614.
30 J. Lee, X. Cheng, J. M. Swails, M. S. Yeom, P. K. Eastman, J. A. Lemkul, S. Wei, J. Buckner, J. C. Jeong, Y. Qi, S. Jo, V. S. Pande, D. A. Case, C. L. I. Brooks, A. D. MacKerell, J. B. Klauda and W. Im, *J. Chem. Theory Comput.*, 2016, **12**, 405–413.
31 K. Vanommeslaeghe, E. Hatcher, C. Acharya, S. Kundu, S. Zhong, J. Shim, E. Darian, O. Guvench, P. Lopes, I. Vorobyov and A. D. Mackerell, *J. Comput. Chem.*, 2010, **31**, 671–690.
32 W. Yu, X. He, K. Vanommeslaeghe and A. D. MacKerell, *J. Comput. Chem.*, 2012, **33**, 2451–2468.
33 H. Bekker, H. Brendsen, E. Dijkstra, S. Achterop, R. Vondrumen, D. Vanderspoel, A. Sijbers, H. Keegstra and M. Renardus, *Phys. Comput.*, 1993, **92**, 252–256.
34 M. J. Abraham, T. Murtola, R. Schulz, S. Páll, J. C. Smith, B. Hess and E. Lindahl, *SoftwareX*, 2015, **1–2**, 19–25.
35 W. Humphrey, A. Dalke and K. Schulten, *J. Mol. Graph.*, 1996, **14**(33–38), 27–28.
36 I. V. Tetko, J. Gasteiger, R. Todeschini, A. Mauri, D. Livingstone, P. Ertl, V. A. Palyulin, E. V. Radchenko, N. S. Zefirov, A. S. Makarenko, V. Y. Tanchuk and V. V. Prokopenko, *J. Comput. Aided Mol. Des.*, 2005, **19**, 453–463.
37 S. H. Choi and T. G. Park, *Int. J. Pharm.*, 2000, **203**, 193–202.
38 H. D. Lu, P. Rummaneethorn, K. D. Ristroph and R. K. Prud'homme, *Mol. Pharm.*, 2018, **15**, 216–225.
39 X. Pan, H. Wang, C. Li, J. Z. H. Zhang and C. Ji, *J. Chem. Inf. Model.*, 2021, **61**, 3159–3165.
40 Y. Sun, P. L. O. Filho, J. C. Bozelli, J. Carvalho, S. Schreier and C. L. P. Oliveira, *Soft Matter*, 2015, **11**, 7769–7777.
41 R. A. Ivanov, O. A. Soboleva, S. A. Smirnov and P. A. Levashov, *Russ. J. Bioorganic Chem.*, 2015, **41**, 260–265.
42 K. Garajová, A. Balogová, E. Dušeková, D. Sedláková, E. Sedlák and R. Varhač, *Biochim. Biophys. Acta, Proteins Proteomics*, 2017, **1865**, 281–288.
43 J. Held and S. van Smaalen, *Acta Crystallogr., Sect. D: Biol. Crystallogr.*, 2014, **70**, 1136–1146.
44 K. Fujiwara, S. Ebisawa, Y. Watanabe, H. Fujiwara and M. Ikeguchi, *BMC Struct. Biol.*, 2015, **15**, 21.
45 C. Jones, B. Mulloy and A. H. Thomas, *Analysis of Polypeptide and Protein Structures Using Fourier Transform Infrared Spectroscopy*, Humana Press, New Jersey, 1993, vol. 22.
46 K. Kuwajima, *Biomolecules*, 2020, **10**, 407.
47 L. Förster, *J. Biol. Chem.*, 1975, **250**, 3738–3745.
48 F. Desantis, M. Miotto, L. Di Rienzo, E. Milanetti and G. Ruocco, *Sci. Rep.*, 2022, **12**, 12087.
49 H. Dong, A. Mukaiyama, T. Tadokoro, Y. Koga, K. Takano and S. Kanaya, *J. Mol. Biol.*, 2008, **378**, 264–272.
50 J. W. Bye and R. J. Falconer, *Protein Sci. Publ. Protein Soc.*, 2013, **22**, 1563–1570.
51 A. P. Yakimov, A. S. Afanaseva, M. A. Khodorkovskiy and M. G. Petukhov, *Acta Nat.*, 2016, **8**, 70–81.
52 L. Zhong and W. C. Johnson, Jr, *Proc. Natl. Acad. Sci. U. S. A.*, 1992, **89**, 4462–4465.

© 2024 The Author(s). Published by the Royal Society of Chemistry